

A redshift survey towards the CMB Cold Spot

M.N. Bremer¹, J. Silk², L.J.M. Davies¹, & M.D. Lehnert³

¹*H H Wills Physics Laboratory, Tyndall Avenue, Bristol, BS8 1TL, UK*

²*Department of Physics, Denys Wilkinson Building, Keble Road, Oxford, OX1 3RH, UK*

³*Laboratoire d'Etudes des Galaxies, Etoiles, Physique et Instrumentation GEPI, UMR8111, Observatoire de Paris, Meudon, 92195 France*

Accepted . Received ; in original form

ABSTRACT

We have carried out a redshift survey using the VIMOS spectrograph on the VLT towards the Cosmic Microwave Background cold spot. A possible cause of the cold spot is the Integrated Sachs-Wolfe effect imprinted by an extremely large void (hundreds of Mpc in linear dimension) at intermediate or low redshifts. The redshift distribution of over seven hundred $z < 1$ emission-line galaxies drawn from an I -band flux limited sample of galaxies in the direction of the cold spot shows no evidence of a gap on scales of $\Delta z \gtrsim 0.05$ as would be expected if such a void existed at $0.35 < z < 1$. There are troughs in the redshift distribution on smaller scales ($\Delta z \approx 0.01$) indicating that smaller scale voids may connect regions separated by several degrees towards the cold spot. A comparison of this distribution with that generated from similarly-sized subsamples drawn from widely-spaced pointings of the VVDS survey does not indicate that the redshift distribution towards the cold spot is anomalous or that these small gaps can be uniquely attributed to real voids.

Key words: Cosmic Microwave Background, galaxies: distances and redshifts, large-scale structure of the Universe

1 INTRODUCTION

A major triumph of modern physics is the measurement and explanation of the Cosmic Microwave Background (CMB) fluctuation spectrum (e.g. Bennett et al., 2003). Encoded within the pattern of fluctuations from constant temperature on the sky are the signatures of the makeup of the Universe. The amount of baryons, matter, dark energy within the Universe, when and how reionization occurred, and the power spectrum of initial fluctuations can all be inferred either from the properties of these fluctuations alone or in combination with other measurements.

The “concordance cosmology”, based strongly on Λ CDM is extremely successful in explaining CMB anisotropies on small angular scales. However, there are clear anomalies on larger angular scales which pose potential problems for our understanding of the evolution of structure at the most fundamental levels. The most striking anomaly is the presence of an apparent cold spot in the Wilkinson Microwave Anisotropy Probe (WMAP) CMB data in the southern hemisphere (Vielva et al., 2004; Cruz et al., 2005; Spergel et al., 2007). This region of decreased temperature ($\Delta T/T \sim -10^{-5}$) extends over an angular scale of $5\text{--}10^\circ$ (Figure 1). The cold spot has a less than 2 per cent probability of being generated as part of a Gaussian fluctuation spectrum (Cruz et al., 2007a).

Assuming that the cold spot is not a statistical artifact, or produced as a result of the way the data has been analysed (e.g. Zhang & Huterer, 2009), determining the nature of the cold spot is crucial to our understanding of the growth of structure. Either it is intrinsic

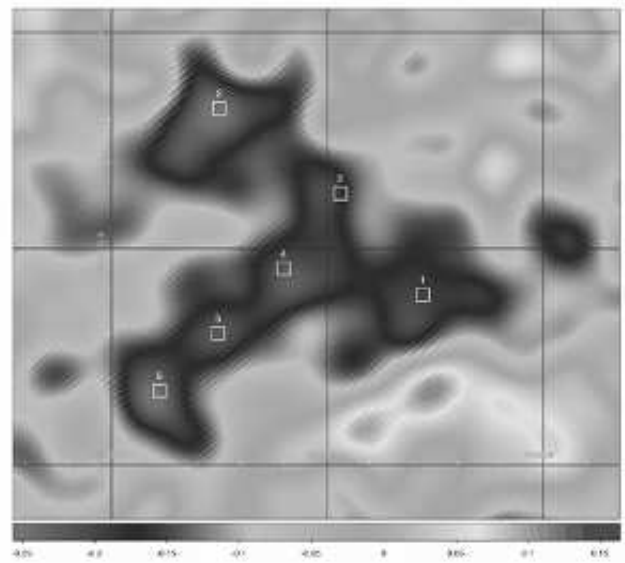


Figure 1. The six spectroscopic field centres overlaid on the WMAP ILC temperature map of the cold spot region. The pointing centres are: (1) 03:28:51 -21:03:54, (2) 03:10:00 -16:45:44, (3) 03:21:13 -18:43:15, (4) 03:15:57 -20:27:23, (5) 03:09:53 -21:57:24 and (6) 03:04:29 -23:17:10

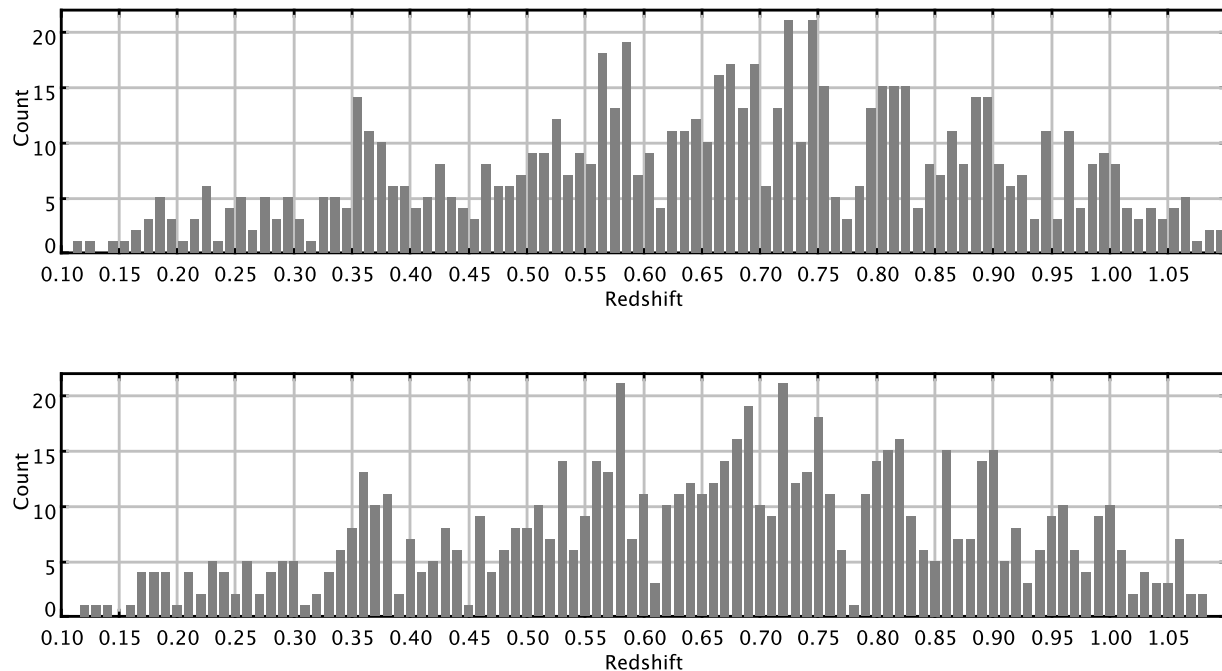


Figure 2. The redshift distribution of the sources in the six fields. Each bin has a width of 0.01 in redshift and the distribution is displayed twice, the second time with the the binning offset by half a bin width. The expected signature of a self-compensating void large enough to produce the cold spot temperature decrement through the ISW effect is an absence of redshifts across several consecutive bins and sharp spikes in the distribution at either edge of the gap. No such feature is seen.

to the CMB itself or is imposed by a foreground structure along the line of sight to the CMB. Either way, there are important implications for our understanding of structure evolution. In the first instance, an intrinsic origin points to extra physics (such as textures or defects, Cruz et al., 2007b, 2008; Durrer 1999) or non-standard inflation (*e.g.* Peebles 1997) influencing the behavior of the early Universe.

A Galactic origin for a foreground source of the cold spot appears to be ruled out by its spectrum (Cruz et al., 2006). If the cold spot is a secondary CMB anisotropy caused by modulation of the CMB signal as it passes through an intervening massive structure, there is only one possible cause. An extremely large void of scale $\sim 200h^{-1}$ Mpc could cause the signal through the Integrated Sachs Wolf (ISW) effect (Inoue & Silk 2006). As the CMB photons pass through such a void, over their transit time the gravitational potential of the void evolves as the void expands leading to a net redshift of the photons and hence cooling of the spectrum at that point in the sky. The size of the void is set not just by the angular size of the cold spot, but also by the light travel time across the void necessary to induce an ISW signal of this magnitude. Any void must be at $z < 1$ as at later times the increasing influence of the cosmological constant on the expansion of the Universe enhances the ISW signature of the void.

We have carried out a redshift survey of galaxies selected from six patches of sky separated by $\sim 1 - 2^\circ$ towards the CMB cold spot in order to search for the signature of an extremely large void capable of producing a large enough ISW signal to account for the CMB feature. Assuming galaxies in such a structure have bias factors similar to those found in typical voids, this structure should be largely empty of galaxies, particularly those around M^* which

dominate the galactic mass distribution. Given its extraordinary size (2-300 Mpc, of order 5-10 percent the distance back to $z \sim 1$), it should leave a clear gap of $\Delta z \sim \text{few} \times 0.01$ in the redshift distribution towards the cold spot depending upon the exact size and redshift of the void.

2 OBSERVATIONS AND DATA REDUCTION

Six separate pointings towards the cold spot were imaged in the *I*-band using VIMOS (LeFevre et al. 2003) on the VLT in service mode between August and October 2008 (ESO service run 082A-0367(A)). The six pointings, shown in figure 1 were chosen to sample areas within the region defined as the cold spot in the WMAP ILC data while avoiding optically bright objects. The data were obtained in photometric conditions with seeing of typically 0.8 arc-seconds. Five dithered exposures totaling 1400 seconds were obtained in each pointing. The data pipeline bias subtracted and flat-fielded the images. Each image was then de-fringed. The five images for each detector quadrant of each pointing were aligned and combined into a final image. A catalogue of all of objects in each image was obtained using SExtractor (Bertin & Arnouts 1996) and the zero-point appropriate for each night was applied. The number counts in the catalogues typically turned over between $24.3 < I < 25$.

These catalogues were then used to design the spectroscopic masks. As the coordinates used for VIMOS mask design are defined through the *R*-band filter, the coordinates in the catalogues were transformed using a (first order) shift and stretch in each of X and Y, determined by a comparison of positions of common objects

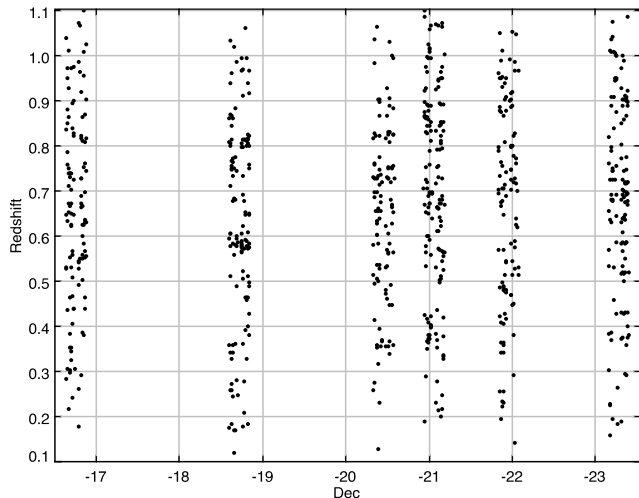


Figure 3. A plot of the Declination and redshift of each source contributing to figure 2. There is no coherent large gap in the redshift distribution common to a subset of the fields that could be attributed to a void large enough to produce the cold spot signature.

in the I -band images and a reference R -band image. Stretches were typically less than a pixel (0.2 arcsec) across an entire quadrant. A subset of objects with $21.5 < I < 22.8$ were selected from these catalogue as input into the VMPS mask-making software (Bottini et al. 2005). Two sets of masks were made for each pointing with between 41 and 70 slits on each quadrant. In total, 2768 objects were essentially randomly targeted for spectroscopy from a total sample of just over 8600 objects in the magnitude range.

Spectroscopic observations were carried out through these masks from November 2008 to February 2009 and during October 2009 (ESO service run 082A-0367(B)). Each mask was observed for 9900 seconds split into 9 exposures with the objects moved along the slits between them. Slits were 1 arcsecond wide and at least 8 arcseconds long. The LR-red grating along with the OS-red order sorting filter was used to give a spectral coverage between 5500 \AA and 9500 \AA . Strong fringing beyond $\sim 7600 \text{ \AA}$ limited the utility of the red part of the spectra. The resolution of the final spectrum was typically $R = 210$ and this was sampled by at least three spectral pixels.

The data were reduced using a bespoke IDL-based pipeline. Each frame was bias subtracted and flat-fielded. Each spectrum within a frame was then sky-subtracted and resampled onto a common wavelength scale. The nine separate exposures for a given mask were then combined and the sky subtraction re-performed to remove any remaining residual sky emission. The multiplexed design of the spectrograph is such that the zeroth-order spectra of some slits fall onto the main first-order spectra of another. This results in either a region of the spectrum with extremely high noise, or an apparent broad emission line in either the sky or on the main object if the compressed zeroth-order spectrum of the other object falls onto that of the main target. These regions were automatically flagged to avoid misleading results.

The spectrum of each object was then optimally extracted from each two-dimensional spectrum. Its wavelength calibration was double-checked by cross-correlating the slits wavelength-calibrated sky spectrum (which was propagated through the pipeline) to a reference sky spectrum. Cases where there were differences of more than 2 \AA were noted. The spectrum was multiplied

by the standard spectral response for the instrument configuration which gave a sufficiently good spectrophotometric calibration for the purposes of redshift determination

Each spectrum was examined by eye. For the purposes of this project redshifts were only assigned for objects with emission lines. Each object was given one of four classifications: (1) secure redshift, (2) very probable redshift (3) possible redshift and (4) no redshift. In the first case multiple emission lines or a clear line plus other spectral features needed to be present. Typically this would be the [OIII] doublet in combination with the $H\beta$ line, or an [OII] line in combination with [NeIII] or CaH&K. Very rarely the $H\alpha$ /NII lines were identified along with the [SII] doublet. In the second case either a strong single line was detected or a second potentially confirming feature was present but compromised by fringing or large sky variation in the red. Based on published equivalent width distributions and the relative volumes probed at $z < 0.2$ and $z > 0.75$ (where $H\alpha$ and [OII] could be confused given the resolution of the spectra), single clear lines were attributed to [OII] rather than $H\alpha$. In the third case a line was detected, but attribution was considered insecure as the strength of the line was insufficient (*e.g.* the line could plausibly be the strongest of the [OIII] doublet lines while leaving the weakest undetected). For the following we only consider the highest two classifications. The spectral resolution was such that centroided wavelengths of individual lines from these objects could be determined to an accuracy of better than 10 Angstroms (so redshifts to better than 0.0015 in the absence of other systematic effects).

In total 750 objects (just under 10 per cent of the total flux limited sample) were classified as having secure or very probable redshifts, 734 of these at $z < 1.1$. The highest redshift object was a quasar at $z = 4.614$. Most objects at $z < 0.5$ were primarily identified through their [OIII] emission, and those at $0.5 < z < 1.1$ primarily from [OII] emission. Although these could in principle be identified from [OIII] emission out to $z \sim 1$, the strong fringing and relatively poor red sensitivity of the detectors meant that the [OIII] doublet was not the primary means of redshift confirmation beyond $z \sim 0.5$.

3 REDSHIFT DISTRIBUTION

The redshift distribution of the 734 objects at $z < 1.1$ is presented in figure 2. The distribution is shown for a bin size of $\Delta z = 0.01$ and duplicated having shifted the bin centres by half a bin width. The signature of a $\sim 300 \text{ Mpc}$ self-compensating void is a gap (or at least a significant lack of redshifts) in a region of size $\Delta z \sim 0.05$ or more, and spikes in the redshift distribution either side of that void, from the “walls” of galaxies that mark out the perimeter of the structure. No such features are seen in this redshift distribution. At $z < 0.35$ the comparatively small number of objects in this distribution may mean that such a structure could be hidden by small number statistics, but out to $z < 1$ where there are several tens or over a hundred of galaxies per 0.1 in redshift, the lack of an obvious gap or strong deficit in the distribution is clear and significant. This data set rules out an unusually large void connecting these six pointings. The redshift distributions of the individual pointings were examined in order to determine whether a large void could be present in a subset, see figure 3. Again, no obvious gap of significant size exists in common across a subset of the pointings.

On smaller scales there are several redshift bins that show a deficit of sources across all pointings in one or both of the binning. Only one pointing contains an object with a redshift in the

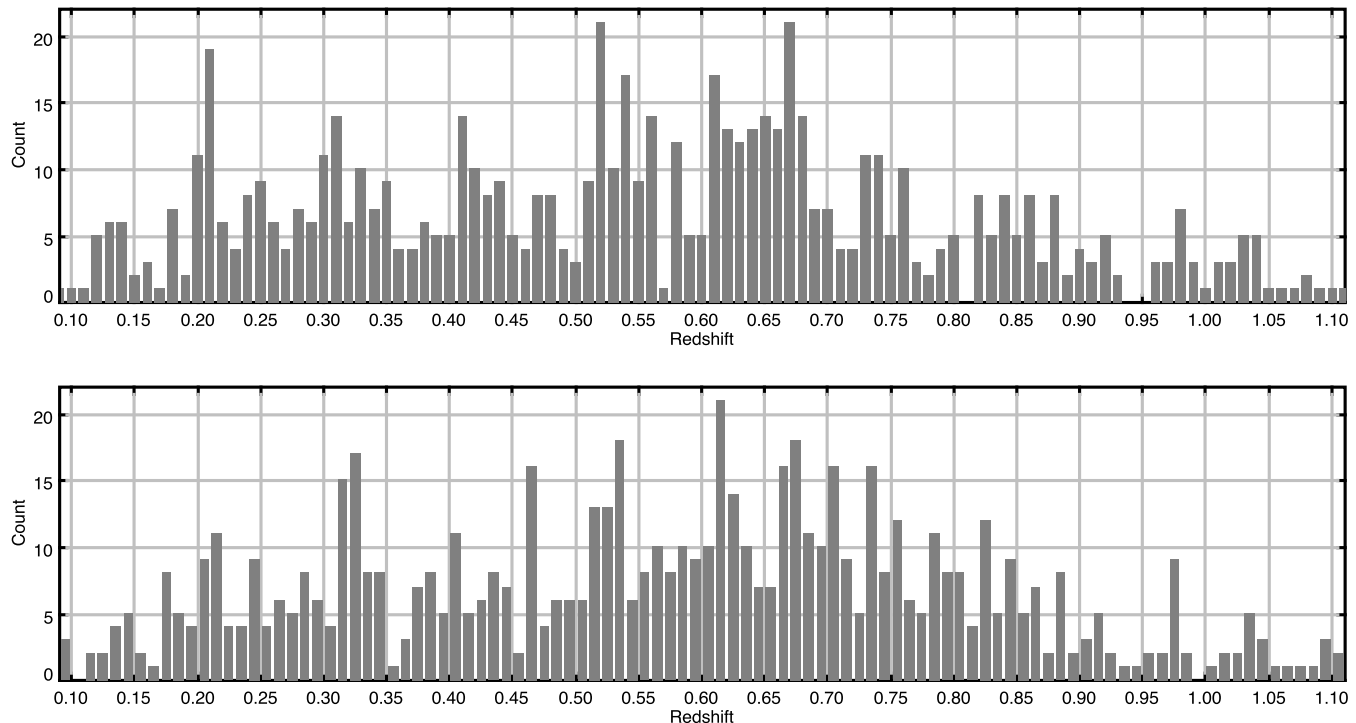


Figure 4. Two example redshift distributions of samples of VVDS sources selected in a similar way and in a similar sample size to our survey and generated from four widely-spaced pointings on the sky. These distributions show redshift bins empty or almost empty of sources, indicating that similar gaps in the redshift distribution of our survey cannot be securely attributed to coherent structures across all or the majority of our pointings. In the case of these VVDS redshift distributions, the distance between the four pointings are so large that no coherent structure can connect them.

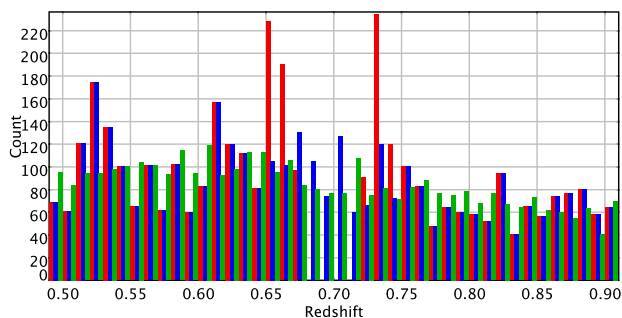


Figure 5. Redshift distribution of reliably-confirmed sources in VVDS (blue). Imposed on this is the faked signature of a huge self-compensating void at $z = 0.7$ (red). In green is the same redshift distribution, but with each redshift randomised by the addition of a number drawn from a Gaussian distribution with $\sigma = 0.05$. The signature of the void is removed by the effective smoothing caused by this randomisation, which is of the same size as typical photometric redshift uncertainties.

range $0.775 < z < 0.785$ and so this could potentially represent a coherent void across a large area of sky, albeit one that was a sheet-like system oriented in the plane of the sky. However, it could also be that this deficit is purely down to the statistics and there is no coherent structure connecting the pointings. To test for this we can generate a comparison sample from spectroscopy of VVDS objects. This spectroscopy was obtained using VIMOS in essentially the same configuration as was used for our survey.

The publicly available VVDS data includes spectroscopic catalogues for three completely independent pointings on the sky separated by tens of degrees (VVDS-CDFS, VVDS-DEEP and VVDS-F22), with spectroscopy in all three regions reaching to at least $I_{AB} = 22.5$ (Lefevre et al. 2004,2005). We selected four areas the size of our individual points, one each from VVDS-CDFS and VVDS-DEEP and two (separated by over a degree) from the larger area VVDS-F22 field. We selected 175 galaxies from each of these four areas, drawn from sources flagged as either > 90 per cent secure redshifts or single line redshifts, the closest match to our selection. We repeated this process several times in order to generate sample redshift surveys with approximately the same number and quality of redshifts as in our survey, albeit drawn from four as oppose to six patches of sky. Three of the four patches are so far apart no coherent 3-dimensional structure could connect them. Of the two that were closer together, there was no expectation of such a structure connecting them, the posited void towards the cold spot ought to be a unique structure on that scale.

Examples of redshift distributions for these samples are plotted in Figure 4. As the redshifts for the VVDS survey are generated initially by an automatic pipeline, the overall shape of the distribution is slightly different to that of ours. This is not significant for our purposes. What is clear is that the redshift distribution of samples drawn from essentially random areas of sky also show empty or near empty redshift bins on scales of $\Delta z = 0.01$. As these are widely-separated fields, these cannot represent true spatially-coherent structures that connect the individual fields, but must simply reflect the statistical variation in the redshift distribution for multiple-field surveys of this size. Given that the kinds of objects targeted in these samples are comparable to those in our

survey, those gaps that are observed in our cold spot redshift distribution cannot be securely attributed to real voids that extend over several of the pointings in our survey.

4 DISCUSSION

The area of sky towards the cold spot has been examined photometrically in several wave-bands other than in the mm-wave in order to search for the signature of a super-void. Rudnick et al (2007) claimed that there is a 25-40 per cent deficit of NRAO VLA Sky Survey (NVSS) sources towards the cold spot and McEwen et al. (2007) demonstrated that the spatial correlation between the NVSS number counts and fluctuations in the WMAP data are strongly influenced by the cold spot area. This is puzzling given the expected redshift distribution of NVSS sources (*e.g.* Raccanelli et al. 2008, Brookes et al. 2008), which is broad and peaks at $z \sim 1$. Any void at $z < 1$ and with a size of $\Delta z \sim 0.1$, even if empty of radio sources and non-compensating for these objects, should depress the number counts towards the void by only a few per cent given the volume of the void and the effective volume probed by NVSS (see also Smith & Huterer 2008).

Conversely, a deep optical imaging survey carried out by Granett, Szapudi & Neyrinck (2009) showed no evidence for a super-void towards the cold spot. Using photometric redshifts derived from g, r, i, z imaging of seven fields within the cold spot region (their pointings A, C and D cover our pointings 6, 2 and 4, and their F & G partially contain our 3 and 1), they claimed to rule out any 200 Mpc void between $0.5 < z < 0.9$. While this agrees with our spectroscopic measurements, we note that attempting to identify a self-compensating void with photometric redshifts which have uncertainties larger than the expected void signal is challenging. This assumes that the uncertainties in photometric redshifts can be fully captured by Gaussian-like error kernels. In reality, while photometric redshifts can be calibrated against the spectroscopic redshifts of objects amenable to spectroscopy, it is not clear that those objects unsuccessfully targeted by spectroscopy (often, as in our case the majority of the targeted objects) follow this calibration. Thus photometric redshift uncertainties could be considerably larger than those characterised from a simple comparison to the successful spectroscopy.

To illustrate the difficulty of using photometric redshifts to probe a putative large self-compensating void, we took the spectroscopic redshifts of all $I_{AB} < 22.5$ VVDS sources with reliable or single-line redshifts (over 7300 objects at $z < 1.4$), changed the redshifts of sources at $0.675 < z < 0.725$ to be at the limits of this range, thereby simulating a self-compensating void with $\Delta z \sim 0.05$. The redshifts were then randomized by shifting each by a random number drawn from a Gaussian distribution of width $\sigma = 0.05$, simulating the statistical uncertainties of photometric redshifts (but ignoring the systematic effect noted above). Figure 5 shows the three redshift distributions: the original VVDS distribution, the same but with the imposed fake void, and then this distribution with the simulated photometric uncertainties. As can be seen, even a broad, sharp void, one with the strongest possible signature for any cold spot, produces no discernible signal in the ‘‘photometric’’ redshift distribution because of the smoothing effect of the uncertainties.

Given the ambiguities of the photometric treatments, the advantage of the spectroscopic approach used here is clear. Our results show no evidence of a void connecting the six pointings towards the cold spot that is large enough to generate the cold spot

through the ISW effect. Given the overall redshift distribution of the galaxies with confirmed redshifts, it is possible that such a void could exist at $z < 0.35$ and with typically only 1-4 sources per $\Delta z = 0.01$ bin in the absence of a void, we would not be sensitive to it. Any future spectroscopic analysis of this area of sky should concentrate on the region at $z < 0.5$. The amplitude of the secondary CMB fluctuation cold spot in the CMB is 7 ± 3.10^{-5} (Cruz et al. 2007b), and if due to the Rees-Sciama effect, varies as the cube of the void radius. Hence the uncertainty in cold spot amplitude at specified angular extent translates into roughly a 15 per cent uncertainty in redshift. Consequently while any void is unlikely to be at $z < 0.5$, this possibility cannot be excluded.

Could we have missed a large void at $0.5 < z < 1$ through the placement of our fields? Our fields were chosen based on the WMAP ILC III map of the cold spot region and cover several per cent of the region with a decrement larger than $100 \mu\text{K}$. If any void had a covering (and filling) factor of less than 100 per cent in this region and our field placings were essentially random within this, then there is a possibility that we could have missed the void. The covering factor cannot be much below 50 per cent as the ISW decrement is directly proportional to the covering factor. For a given signal, any decrease in the covering factor would have to be compensated for by an increased depth to a void in the line-of-sight, leading to potentially implausible geometries for the structure. If an under-density towards the cold spot was made up of several smaller voids with a total covering factor of 50 per cent rather than a single structure, the combined ISW effect from these will produce a far smaller (and therefore undetectable) temperature decrement than a single large void, and so such a scenario is very unlikely. Given the arrangement of our fields across the cold spot region, it is difficult to see how all or even a majority could have missed a single large system.

Our results indicate a large void at $0.5 < z < 1$ is unlikely to have generated the CMB cold spot temperature decrement through the ISW effect. Either such a void is at considerably lower redshift than expected, or there is some other explanation for the cold spot, one possibly involving new physics or a different analysis of current and future CMB data.

5 ACKNOWLEDGMENTS

This work is based on observations made with ESO Telescopes at the La Silla and Paranal Observatory under programme ID 082-0367. Extensive use was made of the STILTS and TOPCAT software packages (Taylor 2005).

REFERENCES

- Bennett et al. 2003, ApJS, 148, 1
- Bertin E., Arnouts S., 1996, A&AS, 117, 393
- Bottini D. et al., 2005, PASP, 117, 996
- Brookes M. H., Best P. N., Peacock J. A., Röttgering H. J. A., Dunlop J. S., 2008, MNRAS, 385, 1297
- Cruz M., Martínez-González E., Vielva P., Cayón L., 2005, MNRAS, 356, 29
- Cruz M., Tucci M., Martínez-González E., Vielva P., 2006, MNRAS, 369, 57
- Cruz M., Cayón L., Martínez-González E., Vielva P., Jin J., 2007a, ApJ, 655, 11

- Cruz M., Turok N., Vielva P., Martínez-González E., Hobson M., 2007b, *Sci*, 318, 1612
- Cruz M., Martínez-González E., Vielva P., Diego J. M., Hobson M., Turok N., 2008, *MNRAS*, 390, 913
- Durrer R., 1999, *NewAR*, 43, 111
- Granett B. R., Szapudi I., Neyrinck M. C., 2009, *arXiv*, arXiv:0911.2223
- Inoue K. T., Silk J., 2006, *ApJ*, 648, 23
- LeFevre O., et al., 2003, *SPIE*, 4841, 1670
- LeFevre O., et al., 2004, *A&A*, 428, 1043
- LeFevre O., et al., 2005, *A&A*, 439, 845
- McEwen J. D., Vielva P., Hobson M. P., Martínez-González E., Lasenby A. N., 2007, *MNRAS*, 376, 1211
- Peebles P. J. E., 1997, *ApJ*, 483, L1
- Raccanelli A., Bonaldi A., Negrello M., Matarrese S., Tormen G., de Zotti G., 2008, *MNRAS*, 386, 2161
- Rudnick L., Brown S., Williams L. R., 2007, *ApJ*, 671, 40
- Smith K. M., Huterer D., 2008, *arXiv*, arXiv:0805.2751
- Spergel D. N., et al., 2007, *ApJS*, 170, 377
- Taylor M. B., 2005, *ASPC*, 347, 29
- Vielva P., Martínez-González E., Barreiro R. B., Sanz J. L., Cayón L., 2004, *ApJ*, 609, 22
- Zhang R., Huterer D., 2009, *arXiv*, arXiv:0908.3988